

The Summer Indoor Thermal Environment of Evaporative Cooling Air-conditioned Rooms in Public Buildings in Northern Xinjiang, China

Xuana Miao¹, Haofeng Sun², Chang Yang^{3*}

¹School of art, Xi'an University of Architecture and Technology, Xi'an 710055, China

²China University of Geosciences, Wuhan 430074, China

³Engineering Comprehensive Training Centre, Xi'an University of Architecture and Technology, Xi'an 710055, China

*Corresponding Author.

Abstract:

Evaporative cooling air conditioning technology is becoming more and more popular in public buildings in hot and dry plateau areas in China. However, there are few studies on the indoor thermal environment problem caused by new technologies. In this study, field tests were conducted on the summer indoor thermal environment of public buildings in the northern Xinjiang area, China. The test results indicate that the indoor cooling effect of an evaporative cooling system attenuates more sharply along the direction of air supply than in the case of mechanical cooling, and the indoor thermal environment shows more significant variation. This study carries out simulations taking a public building model with a small bay width as the research object. Though simulation; with the bay width and net height of the room fixed, the depths of south- and north-facing rooms are changed in simulations of temperature changes under evaporative cooling air conditioning, and the results are compared with standard requirements for thermal comfort. Finally, the best architectural design form and parameter system for local public buildings using evaporative cooling air conditioning technology in summer is proposed, realizing the use of integrated design to promote the utilization of new renewable energy technology.

Keywords: Northern Xinjiang in China; Evaporative cooling technology; Architectural design parameters; Indoor thermal environment

I. INTRODUCTION

The northern Xinjiang region in China is typical of hot plateau areas and has dry climatic conditions. The region is illustrated in Fig. 1.[1] The difference between the dry-bulb temperature and wet-bulb temperature of the outdoor air in this region reaches up to 14–20 °C and “dry air energy” is abundant,[2] making it a highly suitable region for adaptive evaporative cooling ventilation and air conditioning technology.



Fig 1: Location of northern Xinjiang

At present, research at home and abroad into the application of evaporative cooling air conditioning in buildings mainly focuses on what equipment may be used to improve indoor comfort or minimize energy consumption. John.R.Watt, et al.[3] In combination with the ASHRAE comfort effective temperature diagram method, proposed graphical method for quickly calculating the comfort of direct evaporative cooling air conditioning. Huang Xiang et al. [4]pointed out that buildings using evaporative cooling air conditioning have a better airflow distribution than rooms with conventional mechanical cooling air conditioning and that the indoor thermal and humidity environment is also more comfortable. Through simulation using the TRNSYS platform, Elmetenani et al. [5]found that some buildings in the Bechar region of Algeria have greater energy-saving potential during June–August when direct evaporative cooling air conditioning is used rather than conventional mechanical cooling air conditioning. Taking regional climatic conditions into account, Xu Fangcheng et al. [6-7] achieved the goal of reducing the energy consumption of air conditioning systems and realizing environmental protection with an evaporative cooling air conditioning system or a system combining evaporative cooling and mechanical air conditioning. Di Yuhui[8] proposed an energy consumption analysis index for evaporative cooling air conditioning, the degree-hours of evaporative cooling air conditioning, and concluded on the basis of energy consumption calculations that evaporative cooling air conditioning systems have great energy-saving potential. Research by Xia Qing et al. [9] indicated that evaporative cooling air conditioning could satisfy human needs for thermal comfort while also saving energy.

The studies above lay a theoretical foundation for applying evaporative cooling air conditioning in buildings. However, because heating and ventilation are isolated from architectural design, design principles for the equipment have not been considered from an architectural design viewpoint. In particular, little attention is paid to what heating and cooling equipment should be used in specific types of climate-adaptive buildings or to the differences in the indoor thermal environment caused by this new renewable energy heating and cooling technology versus by conventional heating and cooling methods. However, a lack of tests and analysis of the latter aspect make it difficult to form a targeted optimization strategy for

passive integrated building design systems. With continuous improvements in national living standards, there is a growing need for thermal comfort. If differences in the indoor thermal environment caused by the new technology are not diminished, the promotion and application of this new renewable energy technology will be fundamentally impeded.

This paper, by means of field tests in northern Xinjiang, China, comparative analysis, simulation and optimization based on climate suitability factors, combines the technical conditions for heating and ventilation at the initial stage of architectural design and then solves the problem by starting from the architectural form design parameters and applying the standardized parameter system for architectural design. This targeted design strategy for buildings using evaporative cooling technology is shown to improve the indoor thermal environment and realize the integration of energy conservation and comfort, which can provide a basis for the promotion and application of this technology.

II. METHODOLOGY

2.1 Experimental Program

2.1.1 Field test sites

At present, evaporative cooling air conditioning technology in Xinjiang is mainly installed in public buildings. Therefore, they are taken as the main research objects in this study. Accurate horizontal comparative analysis requires that the test object should have universality and representativeness. According to statistical data (Fig. 2), hotels (guest rooms) and hospitals (inpatient departments) account for the greatest proportion of public building areas in northern Xinjiang, about 29%. Both of these types of public buildings see 24-h use, and in the context of applying new energy sources, the indoor thermal environment indices required by the inhabitants are basically the same. They thus are regarded as the research object in this paper.

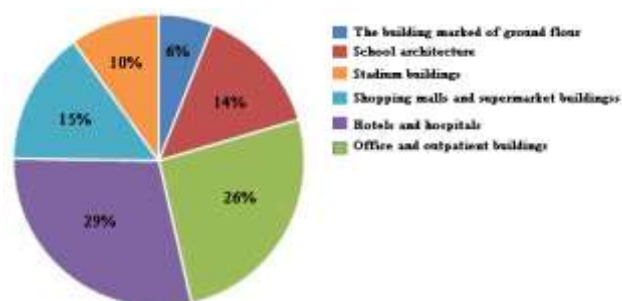


Fig 2: Proportions of different types of public building areas in northern Xinjiang (data obtained from the Statistical Yearbook of Xinjiang)

Through field investigation and research, the Xinrong Building, the Traditional Chinese Medicine Hospital in Xinjiang Autonomous Region, and Haocheng Hotel were selected as the test objects for this study; the case types are detailed in Table 1. All of the rooms have a framed structure, a north–south orientation, two-layer aluminum alloy window frames, and an air-conditioning system. The selected test rooms (standard guest rooms and VIP inpatient wards) are all located on intermediate floors and within intermediate areas so as to avoid ground heat conduction and solar radiation on roofs.

TABLE I. Test Cases

Case	Building name	Location	Orientation	Number of floors	Air conditioning type	Test mode
Case 1	Haocheng Hotel	Turpan	North–south	4	Mechanical air conditioning	Natural ventilation
Case 2	Xinrong building	Urumqi	North–south	17	Mechanical air conditioning	Air conditioning operating
Case 3	Traditional Chinese Medicine Hospital in Xinjiang Autonomous Region	Urumqi	North–south	12	Evaporative cooling air conditioning	Air conditioning operating

2.1.2 Experimental methodology and equipment

Six detection points were arranged inside the test rooms (as shown in Fig. 3) to obtain the temperature and humidity indoors and outdoors. Three indoor detection points were located at the 1/3 and 2/3 points of the cross-section along the depth direction from the air conditioning outlet, respectively, with vertical heights from the ground of 0.5 meters, 1.7 meters, and 3.4 meters. These three locations were set to capture conditions at the sensitive area of the human head in sitting and standing postures and at the height of horizontal air supply from the air conditioning, respectively. Two outdoor detection points were shaded from the wind. The doors and windows were all closed during the testing period, apart from in the case of natural ventilation, when they were kept open, and there was no human activity in the rooms. The test was conducted 24 hours a day from August 1st to August, 9th 2017 with a sampling interval of 20 minutes. During the test period, the weather was clear and there was strong solar radiation. There was no extreme weather for one week before to one week after the test, as is typical of the local climate in summer.

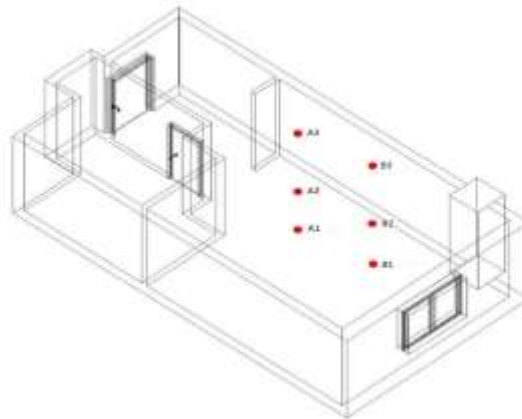


Fig 3: Schematic diagram of detection point arrangement

The environmental factors at each sampling location were measured using a temperature and humidity recording instrument (AZ-8829, AZ Instrument Corp). The temperature range of the instrument is -40 to 85°C , and its resolution is 0.1°C ; the relative humidity range is 0 – 100% , with a resolution of 0.1% . The data recorded were the averages of instantaneous values within one minute. The room size was measured with a laser ranging device (Leica Disto A5) with a detection range of 0 μm and a resolution of 0.01 m. All of the test instruments were calibrated before testing according to relevant specifications and manuals.

2.2 Simulation Scheme

2.2.1 Physical model

In order to improve the current indoor thermal environment of buildings using evaporative cooling air conditioning equipment, this study selects typical types of public buildings for numerical simulation and optimization. Surveying and mapping data and relevant design specifications for guesthouses, hotels and inpatient departments in hospitals are used to establish the dimensions for a common standard room. The “Benchmark model” has length (depth) \times width (bay width) \times clear height dimensions of 7.2 m \times 4.2 m \times 3.6 m, as shown in Fig. 4. The three-dimensional room model is simplified to improve the accuracy and computational efficiency of the simulation. The indoor air conditioning model has the dimensions 0.9 m \times 0.34 m \times 0.2 m, and the standard single bed model has the dimensions 2 m \times 1.2 m \times 0.5 m (two beds). The window is located equidistant from the eastern and western walls, 0.9 m above the ground, and has the dimensions 1.8 m \times 1.5 m \times 0.1 m. According to the habits of indoor air conditioning use, the room is closed to avoid air permeation.

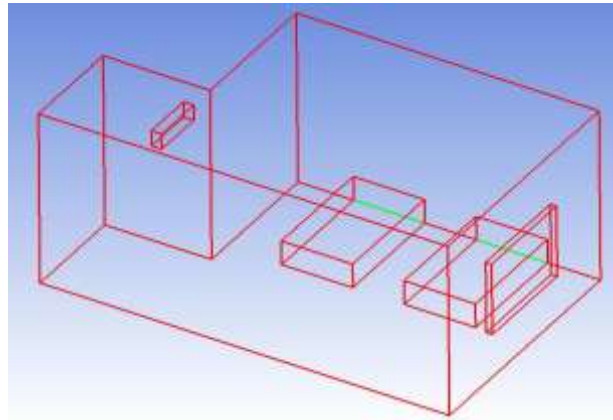


Fig 4: Physical model for public buildings

2.2.2 Mathematical model

Computational fluid dynamics (CFD) calculation models incorporate conservation of mass, momentum, and energy. In this paper, Reynolds time-averaged equations and turbulence models are used to simulate and calculate. Indoor air conditioning in the buildings produces turbulent airflow. Due to the complexity of this flow, the model is simplified, and several assumptions are made: 1) a standard $k-\epsilon$ turbulence model is adopted with consideration given to the effect of gravity; 2) boundary conditions of a constant average wall temperature are used, which considers that the temperature of each wall is constant; 3) the equation for species transport is employed to investigate the relative indoors humidity distribution; 4) indoor airflow flows at a low speed, so it is an incompressible fluid and satisfies the Boussinesq basic assumption; 5) the heat transfer calculation mainly considers the heat transfer inside the fluid without considering coupled heat transfer inside the wall body; 6) energy dissipation due to the effect of viscosity is ignored in the energy equation; 7) the effect of indoor pollutants on air distribution is ignored; 8) the air circulation jet at the air-supply outlet is uniform and stable. [10]

2.2.3 Cell meshing and independence analysis

The self-contained cell generation software in ANSYS 18.1 — ICEM CFD was employed to generate a cell with a hexahedral structure at the highest accuracy currently possible. Fig. 5 showed the variation of the temperature of the center of supply opening at the Z-axis in the three cells. When the number of cells was about 160,000, the temperature difference between the temperature and the other two conditions is very large. When the number of cells was about 160,000, the temperature value was much different from the temperature changes in the other two conditions. When the number of cells was around 400,000 and 670,000, the temperature values have almost the same trend. Therefore, it can be considered that the results of these two conditions are independent of the cell. Based on calculation speed, the number of cells was set to about 400,000. The model meshing results were shown in Fig. 6.

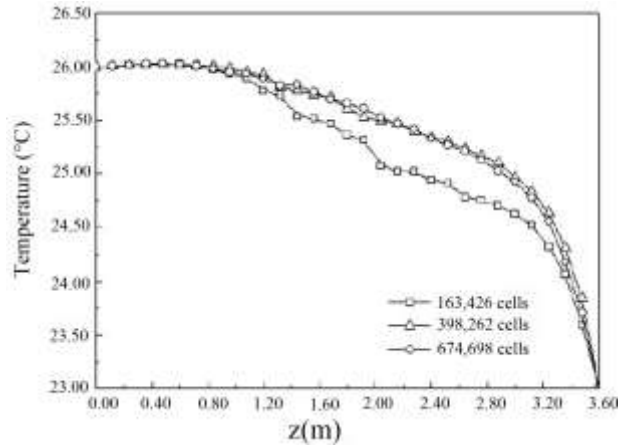


Fig 5: Cell independence analysis

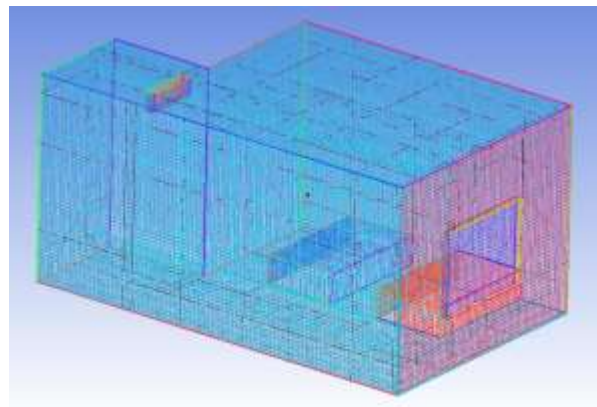


Fig 6: Partition diagram for the cells of the model

2.2.4 Solution

After the flow field is initialized, the computational region is solved iteratively. In this study, the SIMPLE algorithm with standard pressure–velocity coupling is used to conduct discrete solution on the established mathematical model. The low-order (first-order) discretization scheme is used for the initial solution. After the convergence of the first iteration, the high-order scheme (QUICK) is used to continue to solve until the calculation is completed, [11-13] as shown in Table 2.

TABLE II. Discrete Scheme of SIMPLE Algorithm

Step	Pressure	Momentum	Energy	k-equation	ϵ -equation	Diffusion item
Step 1	Standard atmospheric pressure	First-order upwind scheme	First-order upwind scheme	First-order upwind scheme	First-order upwind scheme	First-order central difference

Step 2	Second-order upwind scheme	QUICK scheme	QUICK scheme	QUICK scheme	QUICK scheme	Second-order central difference
--------	----------------------------	--------------	--------------	--------------	--------------	---------------------------------

2.2.5 Simulation condition

The main reason that inhabitants feel uncomfortable in environments cooled by evaporative cooling air conditioning is the differences in temperature and humidity caused by an excessively large room depth. [14-15]Therefore, in the original dimensions of the test building, the bay width and clear height of the rooms are kept invariable. By means of gradually changing the depth of north-facing and south-facing rooms,^[16]simulation and comparative study are conducted on the indoor thermal environment under evaporative cooling air conditioning, as shown in Table 3. 5.1 (6.9) indicates that the room depth is 5.1 meters (except the length of the bathroom). The bathroom is 1.8 meters long, and the other working conditions are the same. 3.9 (5.7) size is according to the specification, the minimum depth of the standard room for the double room. The changes of the depth dimension of the simulation scheme is based on the building modulus as a unit variable (300mm), in order to optimize the transformation.

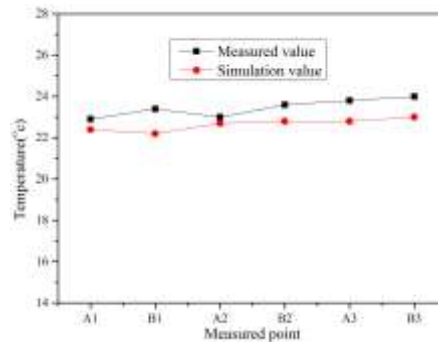
TABLE III. Simulation Scheme

Toward	Width (m)	Net height (m)	Depth (m)
South-facing and North-facing	4.2	3.6	5.1(6.9), 4.8(6.6), 4.5(6.3),4.2(6.0), 3.9(5.7)

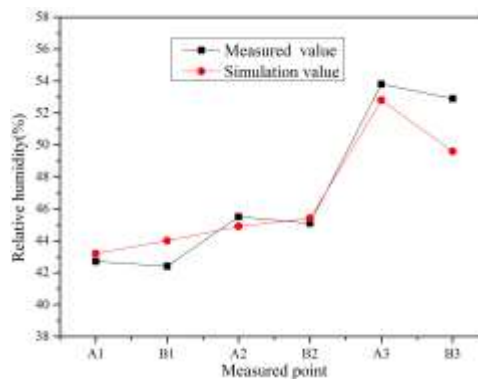
In the simulation, the air conditioning air outlet speed, temperature and relative humidity parameters used the measured value. The simulated boundary condition parameters are measured data. The air supply port of the air conditioner was a Velocity-inlet, and the air supply temperature was 22.5°C and the speed is 0.8 m/s. The exit boundary was the return air outlet of the air conditioner, and set to the pressure-outlet. The temperature of the south facing room was set to 29.85°C, and the temperature of the north facing room was set to 27.35°C. The wall is set to stabilize the wall with a surface roughness of 0.5. The density was set to 1800 kg/m³. The constant pressure specific heat was set to 880 J/(kg·K). The thermal conductivity was set to 0.815 W/(m·K). The wall temperature in the south facing room was set to 26.85 °C, and the wall temperature in the north facing room was set to 24.88 °C. The wall is set to stabilize the wall with a surface roughness of 0.5, and density is set to 1800 kg/m³, and constant pressure specific heat was set to 880 J/(kg·K), and thermal conductivity was set to 0.824 W/(m·K). The south window had a temperature of 31.85°C and the north window had a temperature of 29.35°C. The window was set to a stable window with a surface roughness of 0.4, and density was set to 2500 kg/m³, and constant pressure specific heat was set to 835 J/(kg·K), and thermal conductivity was set to 2.8 W/(m·K).

2.2.6 Experimental verification

In order to verify the accuracy of the numerical simulation results, this paper compared and analyzed the measuring results and simulation results. The measured average temperature was selected as a comparison index. By comparing and analyzing the measured values and simulation values of temperature and relative humidity, the maximum error range is 6.20%, as shown in Fig. 7, This determined the feasibility of the model and simulation settings.



(a) Temperature



(b) Relative humidity

Fig 7: Comparison of simulation and Measured data

III. RESULTS AND DISCUSSION

3.1 Thermal Environment Experiment Comparison

It can be seen from Fig. 8–Fig. 13 that Case 1 provides the worst indoor thermal environment of the three cases, as it is affected most significantly by the outdoor environment, and the amplitude of temperature and humidity fluctuation is greater. The daily mean temperature and relative humidity indoors are 28.8°C and 28.2%, respectively. It is dry and stuffy inside the rooms, but there is a uniform spatial distribution of temperature and humidity. The indoor thermal environment is best in Case 2. The daily

mean temperature and relative humidity indoors are 24.3°C and 48.22%, respectively. The temperature gradient along the vertical direction is slightly greater than along horizontal direction but shows no significant difference since it always fluctuates within 1°C/m. In Case 3, significant differences are seen in the indoor thermal environment. The indoor cooling effect is relatively poor, and the distribution of the thermal environment is uneven. The daily mean temperature and relative humidity indoors are 26.9 °C and 36.8%, respectively, and the average temperature in the hottest period of the afternoon can reach up to 27.1°C. There is an obvious temperature gradient along the depth direction on each horizontal plane, with a temperature difference in the range 2.2–2.5°C, and there is no significant vertical gradient.

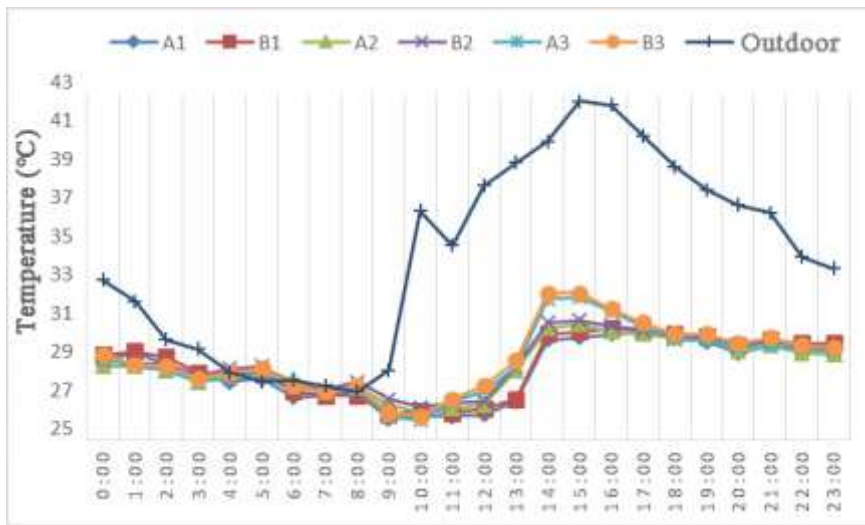


Fig 8: Temperature–time curve for Case 1

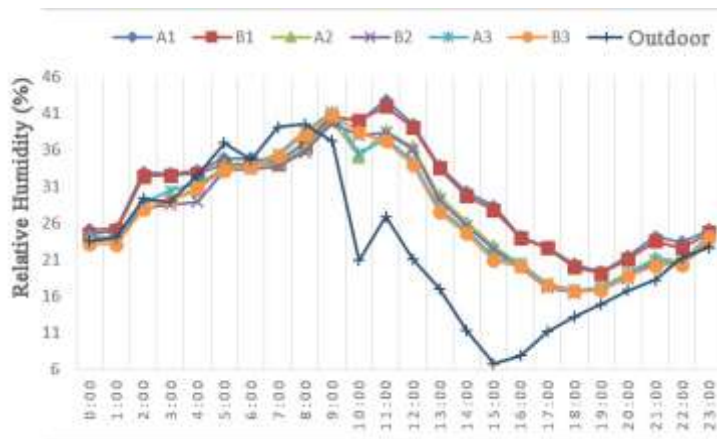


Fig 9: Humidity–time curve for Case 1

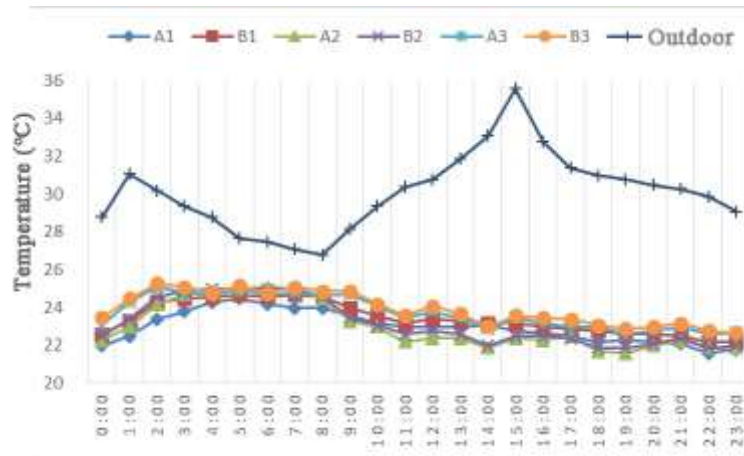


Fig 10: Temperature–time curve for Case 2



Fig 11: Humidity–time curve for Case 2

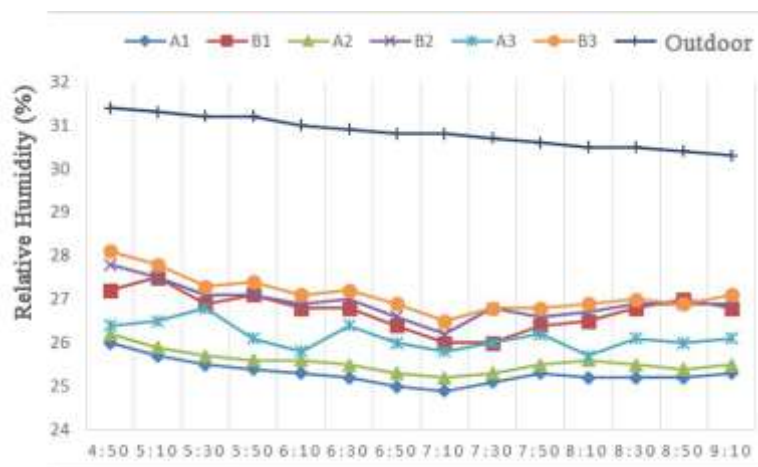


Fig 12: Temperature–time curve for Case 3

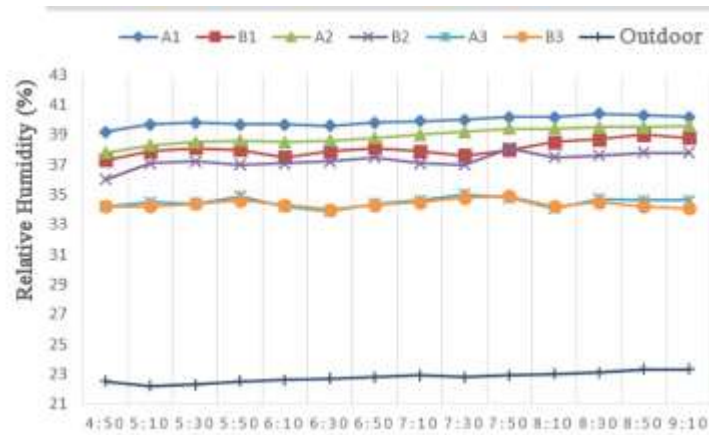


Fig 13: Humidity-time curve for Case 3

3.2 Influence of the Depth on Thermal Environment

The south-facing rooms are taken as the example for discussion of the simulation results for indoor temperature and humidity under different conditions. Because the methodologies for the north- and south-facing rooms are basically the same, the results for the north-facing rooms reported in summary form.

3.2.1 South-facing rooms

As shown in Fig. 14–Fig.16, when the depth is $d=5.1$ (6.9) m, the overall average room temperature is 26.9°C and the maximum temperature difference along the depth direction is 2.2°C , an obvious temperature gradient, and it is stuffy in the room. The average relative humidity in the major activity areas is 36.8%, and the maximum humidity in the horizontal direction appears in the area passed by the jet flow. With increases in height and depth, the humidity first rises slowly and then decreases, with a gradient of about 3-5%.

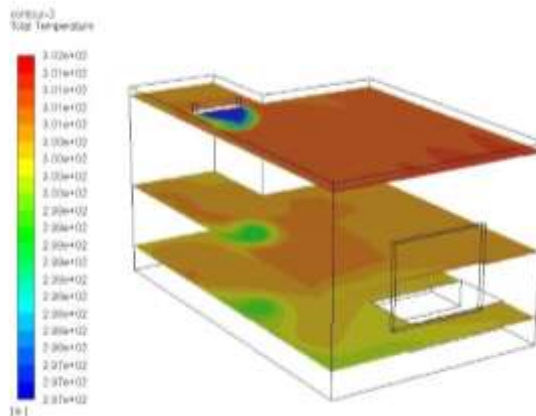


Fig 14: Temperature distribution clouds for $z=0.5$ m/1.7 m/3.4 m

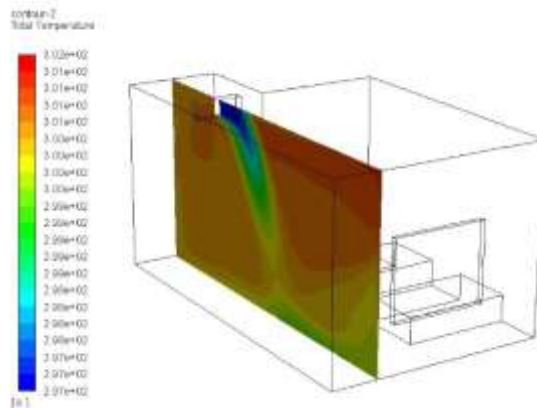


Fig 15: Temperature distribution cloud for $x=1$ m

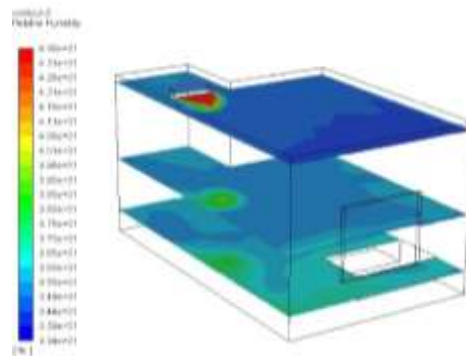


Fig 16: Humidity distribution clouds for $z= 0.5$ m/ 1.7 m/ 3.4 m

As shown in Fig.17–Fig.19, when the room depth is $d=4.8$ (6.6) m, the overall average room temperature under evaporative cooling is 26.1°C , and the maximum temperature difference along the depth direction is 1.7°C . This is again an obvious temperature gradient, and it is stuffy in the room. The average relative humidity in the major activity area is 38.5% , and the maximum humidity in the horizontal direction appears in the area passed by the jet flow. The humidity first rises slowly and then decreases with increase in depth, with a gradient of about $3\text{-}5\%$.

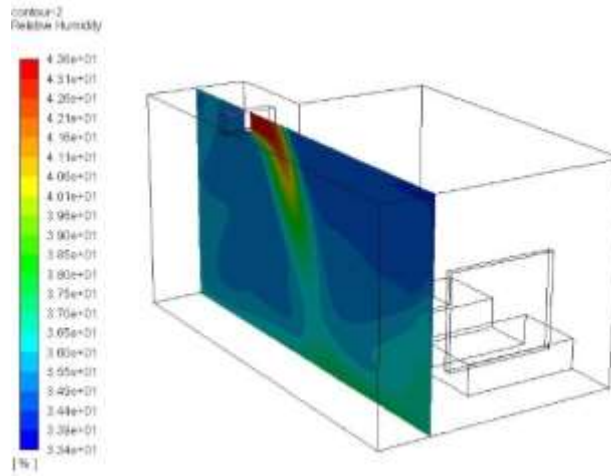


Fig 17: Temperature distribution cloud for z=0.5 m/1.7 m/3.4 m

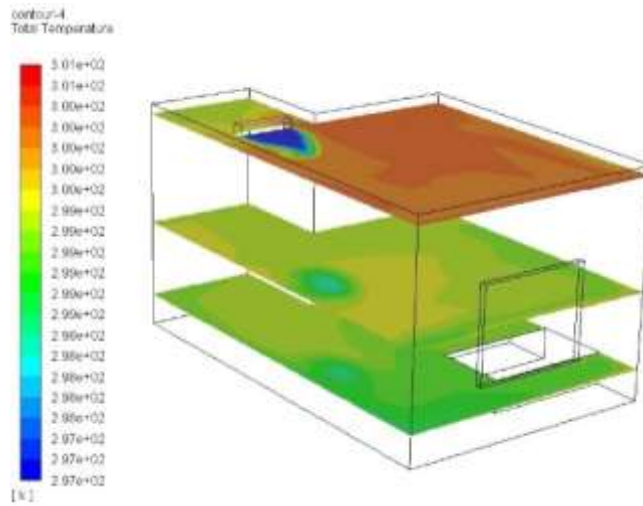


Fig 18: Temperature distribution cloud for x=1 m

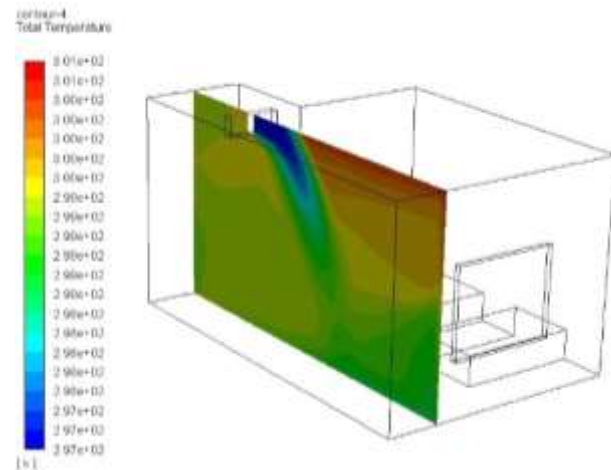


Fig 19: Humidity distribution clouds for z=0.5 m/1.7 m/3.4 m

As shown in Fig. 20–Fig. 22, when the room depth is $d=4.5$ (6.3) meters, the overall average room temperature under evaporative cooling is 25.2°C , and the maximum temperature difference along the depth direction is 1.2°C , indicating that the temperature gradient has decreased to some extent. The average relative humidity in the major activity areas is 39.5%, and the maximum humidity in the horizontal direction appears in the area passed by the jet flow. The humidity first rises slowly and then decreases with increase in depth, with a gradient fluctuating within 2%.

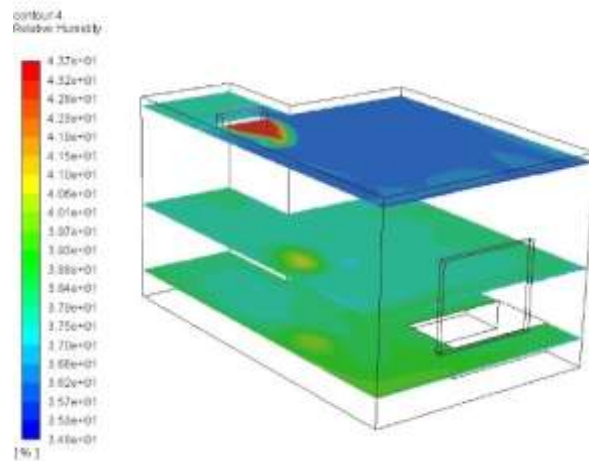


Fig 20: Temperature distribution clouds for $z=0.5$ m/1.7 m/3.4 m

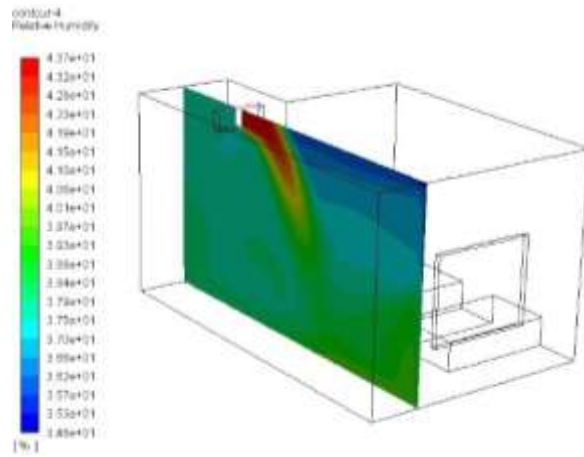


Fig 21: Temperature distribution cloud for $x=1$ m

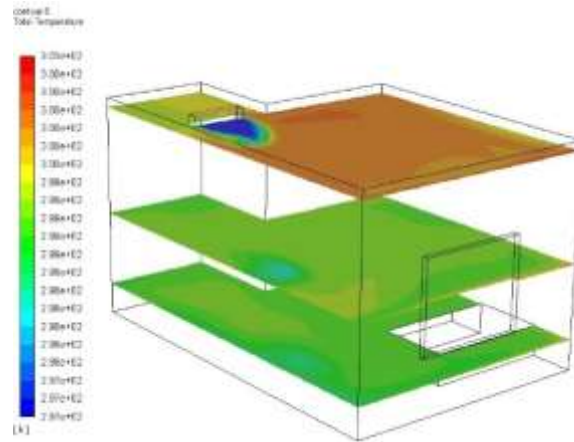


Fig 22: Humidity distribution clouds for z=0.5 m/1.7 m/3.4 m

As shown in Fig. 23–Fig. 25, when the depth is $d=4.2$ (6.0) m, the overall average room temperature under evaporative cooling is 24.8°C , and the maximum temperature difference along the depth direction is 0.7°C , with a temperature gradient of less than $1^{\circ}\text{C}/\text{m}$. The average relative humidity in the major activity areas is 42.7%. The humidity rises slowly and shows no significant variation with an increase in depth in the horizontal direction. According to the “Design Code for Heating Ventilation and Air Conditioning of Civil Building ” GB 50736-2012 and ISO 7730, the temperature and humidity conform to standards for the thermal comfort of the human body.

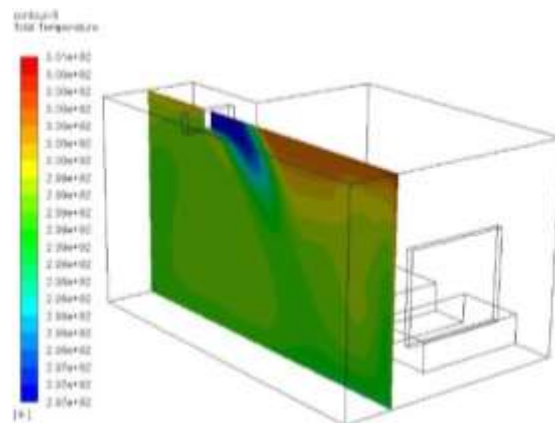


Fig 23: Temperature distribution clouds for z=0.5 m/1.7 m/3.4 m

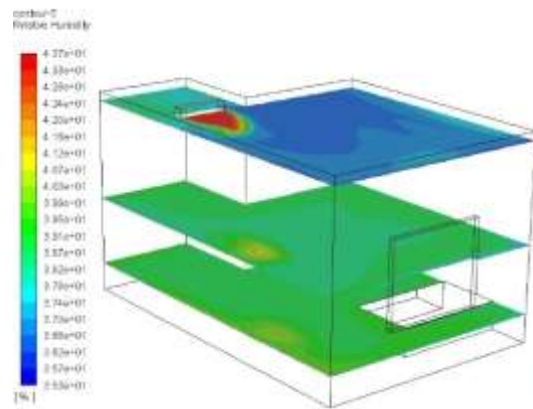


Fig 24: Temperature distribution cloud for x=1 m

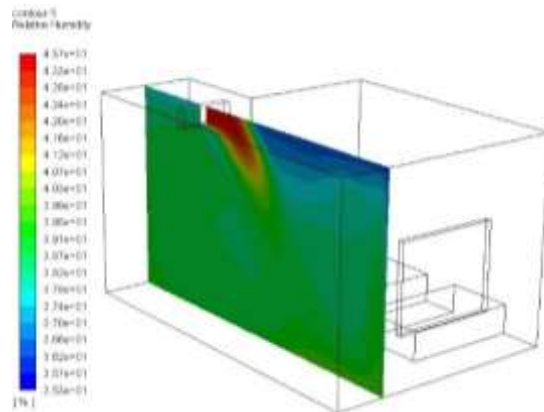


Fig 25: Humidity distribution clouds for z=0.5 m/1.7 m/3.4 m

As shown in Fig. 26–Fig. 28, when the depth is $d=3.9$ (5.7) m, the overall average room temperature under evaporation-cooling is 24.6°C , and the maximum temperature difference along the depth direction is about 0.5°C , with a temperature gradient of less than $1^{\circ}\text{C}/\text{m}$. The average relative humidity in the major activity area is about 45%. The humidity is relatively stable with an increase in depth along the horizontal direction. According to the “Design Code for Heating Ventilation and Air Conditioning of Civil Building” GB 50736-2012 and ISO 7730, the temperature and humidity both conform to standards for the thermal comfort of the human body.

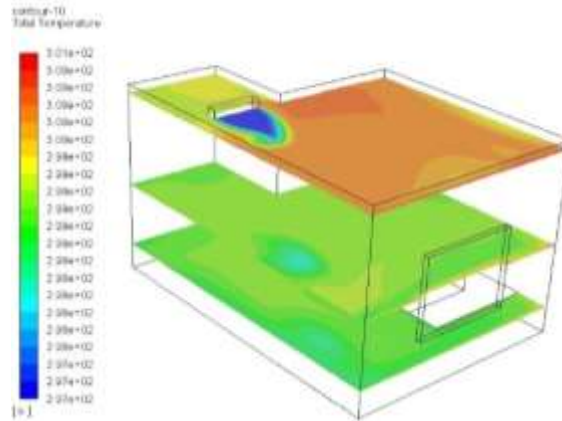


Fig 26: Temperature distribution clouds for $z=0.5$ m / 1.7 m / 3.4 m

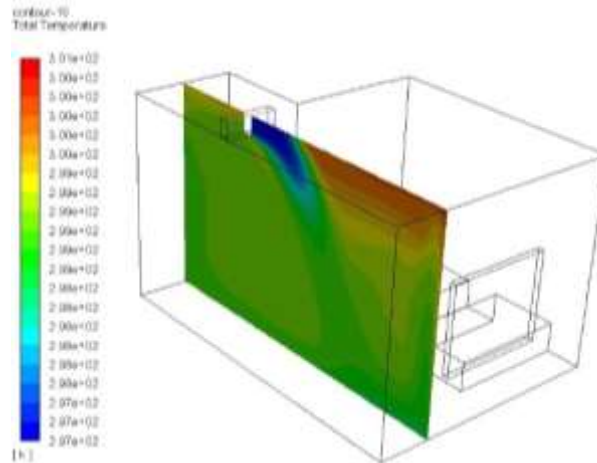


Fig 27: Temperature distribution cloud for $x=1$ m

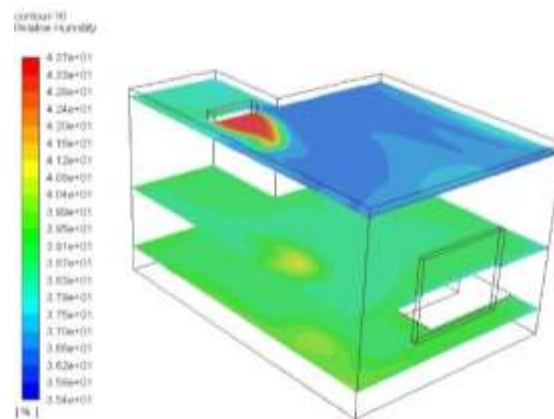


Fig 28: Humidity distribution clouds for $z=0.5$ m / 1.7 m / 3.4 m

3.2.2 North-facing rooms

Simulation results for the temperature and humidity field of north-facing rooms obtained using the same methodologies are shown in Table 4.

TABLE IV Simulation Results for Temperature and Humidity in North-facing Rooms

Room depth (m)	5.1(6.9)	4.8(6.6)	4.5(6.3)	4.2(6.0)	3.9(5.7)
Average temperature (°C)	25.8	25.2	24.6	24.3	24
Temperature gradient along depth direction (°C)	1.6	1.4	0.8	0.5	0.4
Average humidity (%)	38.7	40.2	43.5	45.8	48.2
Humidity gradient along depth direction (%)	3~5	3~5	≤3	≤3	≤3

IV. CONCLUSIONS

The test results indicate that the indoor cooling effect of an evaporative cooling system attenuates more sharply along the direction of air supply than in the case of mechanical cooling, and the indoor thermal environment shows more significant variation. The best room depth range for standard north-south orientated buildings such as guesthouses, hotels, and hospitals in northern Xinjiang, China where evaporative cooling technology is used for cooling in summer has been determined through simulation. In 5.7–6 m-deep south-facing rooms and 5.7–6.3 m deep north-facing rooms with a bay width and clear height of standard design dimensions, the overall average temperature throughout the day can reach up to 24–25°C, and the horizontal and vertical temperature differences are less than 1°C. The overall average relative humidity can reach up to 40–50%, and the humidity difference is small. The above temperature and humidity characteristics can satisfy requirements for the thermal comfort of the human body.

REFERENCES

- [1] GB50736-2012 2012. Design code for heating ventilation and air conditioning of civil buildings. Beijing: China Architecture & Building Press.
- [2] Wu Y C, Huang X, Chu J J, Wang W B, Du D Y. (2017) Thermal comfort analysis of an evaporative cooling air conditioning dormitory in xi 'an area. Building energy efficiency 8: 6-12.
- [3] (United States) John Watt, Er Brown. (2009) Evaporative Cooling Air Conditioning Technical Manual. Huang Xiang, Wu Junmei, et al. Beijing: Mechanical Industry Press.
- [4] Huang X, Liang C H, et al. (2004) Thermal comfort and evaporative cooling air conditioning. Building thermal ventilation 23 (2): 13-17.
- [5] Elmetenani S, Yousfi M L, Merabeti L, Belgroun Z, Chikouche A. (2011) Investigation of an evaporative air cooler using solar energy under Algerian Climat. Energy Procedian 6: 573-582.

- [6] Xu F. C, et al. (2009) Experimental study on evaporative cooling and mechanical refrigeration composite air conditioning unit. HVAC 39 (9): 42-45.
- [7] Xu F C, Huang X, Wu J M. (2007) Technical and economic analysis of two air conditioning systems in an office building in Xi'an. Refrigeration Air Conditioning and Electric Power Machinery 28(118): 39-42.
- [8] Di Y H, Liu J P, Huang X. (2010) Climate Adaptation Area Division of Evaporative Cooling Air Conditioners. HVAC 40.
- [9] Xia Q, Huang X, et al. (2013) Evaporative cooling and indoor thermal comfort in building environment. Refrigeration and Air Conditioning 27(5): 429-432(2): 108-111.
- [10] Sui H. T, Li P F. (2013) CFD dynamic mesh engineering simulation and case study. Beijing: People's postal and telecommunications press.
- [11] He M. (2014) Study on thermal environment of air conditioning condition in student dormitory of a university in Chongqing. Chongqing: Chongqing university, master's thesis
- [12] Huang X, Zheng W H. (2003) Energy saving and purification treatment of all fresh air conditioning system. Xi 'an refrigeration2: 1-5.
- [13] Steeman M, Janssens A, De Paepe M. (2006) Indirect evaporative cooling: interaction between thermal performance and room moisture balance. way 5: 6.
- [14] Steeman M, Janssens, Arnold, DePaepe M. (2009) Performance evaluation of indirect evaporative cooling using whole-building hygrothermal simulations. Applied Thermal Engineering 29 (14): 2870-2875.
- [15] Ankur K, Prabal T, Snjeev J. (2011) Energy savings in a building using regenerative evaporative cooling. Energy and Buildings (43): 581-591.
- [16] Elmetenani S, Yousfi M L, Merabeti L, Belgroun Z, Chikouche A. (2011) Investigation of an evaporative air cooler using solar energy under Algerian Climat. Energy Procedian 6: 573-582.